Fizika Nizkikh Temperatur, 2008, v. 34, No. 10, p. 1072–1080

Index of refraction of a photonic crystal of carbon nanotubes and homogenization of optically anisotropic periodic composites

L.N. Gumen[1] and A.A. Krokhin[2]

[1]*Universidad Popular Autonoma del Estado de Puebla, 21 Sur, #1103, 72160, Mexico*

[2]*Department of Physics, University of North Texas, P.O. Box 311427, Denton, TX, 76203, USA*
E-mail: arkady@unt.edu

Received January 31, 2008

We consider the long-wavelength limit for a periodic arrangement of carbon nanotubes. Using the Fourier expansion method we develop an effective-medium theory for photonic crystal of aligned optically anisotropic cylinders. Exact analytical formulas for the effective dielectric constants for the *E* and *H* eigenmodes are obtained for arbitrary 2D Bravais lattice and arbitrary cross-section of anisotropic cylinders. It is shown that depending on the symmetry of the unit cell photonic crystal of anisotropic cylinders behaves in the low-frequency limit like uniaxial or biaxial optical crystal. The developed theory of homogenization is in a good agreement with existing experimental results for the dielectric tensor of photonic crystals of carbon nanotubes.

PACS: 42.70.Qs Photonic bandgap materials;
41.20.Jb Electromagnetic wave propagation; radiowave propagation;
42.25.Lc Birefringence;
78.67.Ch Nanotubes.

Keywords: photonic crystal, carbon nanotubes, dielectric constants.

Introduction

Photonic crystals have been introduced after the publication by Yablonovitch and Gmitter [1], where the presence of a photonic band gap was experimentally demonstrated. Since that the photonic band gap materials have found numerous applications in optoelectronics and photonics [2]. A photonic crystal is an artificial structure with periodic arrangement of «atoms» — dielectric (or metallic) objects of arbitrary form with dielectric constant ε_a, imbedded in a homogeneous background material with dielectric constant ε_b. Due to diffraction of electromagnetic waves at the boundaries between two constituents the band gap (or gaps) may open for some types of unit cells if the dielectric contrast $|\varepsilon_a - \varepsilon_b|$ exceeds some critical value. This gives rise to distinct optical phenomena such as inhibition of spontaneous emission [3], high-reflecting omni-directional mirrors [4] and low-loss-waveguiding [2,5]. Photonic crystals with specially engineered nanostructures may exhibit optical properties that do not exist for natural crystals. In this case the artificial photonic crystals are referred to as *metamaterials*. The most known, so far, phenomena attributed to the metamaterials are the anomalous Doppler effect [6], negative index of refraction [7], and huge optical anisotropy [8–10]. Only the anomalous Doppler effect manifests itself at the frequencies close to the band edge. Unlike this, the other two phenomena may be observed at much lower frequencies. This means that the photonic crystals can be also employed in the frequency region well below the gap, where the wavelength covers many periods of the structure. Here the periodic medium behaves like a homogenous one and its optical properties can be characterized by effective parameters, like, e.g., the effective index of refraction. The mathematical theory of heterogenous structures in the long-wavelength limit is called the theory of homogenization [11]. Numerous practical applications of photonic crystals made strong impact to the theory of homogenization. During a short period of time the new powerful methods have been developed and many new results have been obtained [8,12–29].

Fabrication of a photonic crystal with the period comparable near-infrared or optical range is a challenging technological problem [2,4]. Carbon nanotubes, being high-quality dielectric nanomaterial with extraordinary mechanical properties, is a promising constituent for fabrication of 2D photonic crystals [30–34]. Due to appropriate relation between dielectric and conductive properties of carbon nanotubes, a triangular lattice of aligned carbon nanotubes exhibits the effect of negative index of refraction [34]. Due to this metamaterial property, photonic crystals of carbon nanotubes may be used in engineering of superlens — optical device that produce images with subwavelength resolution [35]. There are also a lot of possible applications of photonic crystals as traditional optical elements like polarizers, prisms and lenses [2,8,12]. In the latter case the diffractive properties of a photonic crystal are not explored and it serves as an artificial dielectric material with custom-tailored optical characteristics. These characteristics may be quite different from those of natural crystals and give rise, for instance, to unusually large birefringence.

In order to calculate these effective characteristics, we develop an analytic approach to the optical properties of photonic crystals with cylindrical atoms. We are using the term «optical» in the sense that the wavelength of the propagating wave is much larger than the lattice period of the crystal; for natural crystals this condition fits the spectral region up to the ultraviolet [36]. For photonic crystals the lattice constant is, of course, a variable quantity. Therefore, the long-wavelength regime's upper limit may be anywhere between radio waves and the far infrared. In practice, many photonic band-gap materials exhibit a linear dispersion law, for both propagating modes, almost up to the gap frequency. This rather wide region (usually wider than the band-gap) can be considered as the domain of «photonic crystal optics». Due to the linearity of the dispersion law, each mode is characterized by a unique parameter — its effective dielectric constant. It appears in the homogenized solution of Maxwell's equations for the periodic medium, which thus can be replaced by an effective homogeneous medium with effective permittivity

$$\varepsilon_{\text{eff}}(\hat{\mathbf{k}}) = \lim_{k\to 0}\left(\frac{ck}{\omega}\right)^2. \qquad (1)$$

In the general case, this effective parameter depends on the direction of propagation $\hat{\mathbf{k}} = \mathbf{k}/k$ and has tensor structure. The latter property is emphasized for 2D PC's, which are anisotropic uniaxial or biaxial crystals, depending on the symmetry of the unit cell [8,21]. Unlike this, 3D PC's may be isotropic [15].

Optical anisotropy of the photonic crystals studied in Refs. 8, 14, 15, 18–21, 23, 25, 27 is determined by the geometry of the unit cell only. The constituents themselves are considered to be isotropic dielectrics. This is not the case, for example, for a structure of aligned carbon nanotubes arranged periodically in the plane perpendicular to the tubes. Here anisotropy manifests itself at the «microscopic» level, since the nanotubes («atoms» of the photonic crystal) are optically anisotropic. Anisotropy originates from the layered structure of the graphite crystal, which has different dielectric constants along the c axis and in the perpendicular plane. The static values of these dielectric constants are $\varepsilon_{\parallel} = 1.8225$ and $\varepsilon_{\perp} = 5.226$ [37]. The elongated topology and the natural anisotropy of graphite cause the photonic crystals of carbon nanotubes to exhibit large optical anisotropy [30–34]. Three-dimensional PC's with anisotropic dielectric spheres have been studied in Refs. 16. It was shown, that, depending on the symmetry of the unit cell, the anisotropy of the spheres may be favorable for either broadening or narrowing the band gaps.

High anisotropy of 2D photonic crystals may find interesting applications in nanophotonics as it was recently proposed by Artigas and Torner [10]. Namely, the surface of an anisotropic 2D photonic crystal supports propagation of a surface wave predicted by Dyakonov [38]. The surface mode does not radiate and is localized close to the surface due to the interference between the ordinary and extraordinary waves. In natural crystals, it can be hardly observed because of the low anisotropy. Since it is a surface wave with very low energy losses, the Dyakonov wave may replace surface plasmons in the near-field optics and integrated photonic circuits. At the same time application of optically anisotropic substrates leads to essential increase of the propagation length of surface plasmons, thus, giving rise to higher efficiency of plasmonic devices [39]. These and other examples show that dielectric materials with high optical anisotropy is on demand in modern optoelectronics.

Here we develop a theory of homogenization for periodic heterogeneous dielectric medium with intrinsic anisotropy and apply the results for calculation of the effective dielectric tensor of a photonic crystal of carbon nanotubes.

2. Method of plane waves

We consider a 2D periodic structure of dielectric cylinders with their axes parallel to z and whose cross section can have an arbitrary shape (Fig. 1). The cylinders are imbedded in a dielectric matrix. A 2D PC supports propagation of two uncoupled modes with either E polarization (where the vector **E** is parallel to the cylinders, representing the TE mode), or H polarization (in this case the vector **H** is parallel to the cylinders, representing the TM mode). The background material is an isotropic dielectric with permittivity ε_b and the cylinders are rolled up from an anisotropic dielectric sheet characterized by a tensor $\hat{\varepsilon}^{(a)}$. For carbon nanotubes, this tensor has two different

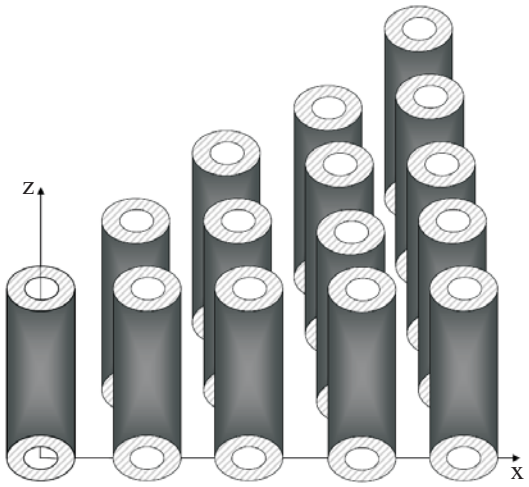

Fig. 1. Periodic arrangement of dielectric cylinders. We assume an arbitrary cross-sectional form of anisotropic cylinders, arbitrary Bravais lattice, and filling fraction of the cylinders.

eigenvalues, and in cylindrical coordinates is represented by a diagonal matrix with elements $\varepsilon_{\theta\theta}^{(a)} = \varepsilon_{zz}^{(a)} = \varepsilon_\perp$ and $\varepsilon_{rr}^{(a)} = \varepsilon_\parallel$. As a whole, the periodic inhomogeneous dielectric medium is characterized by the coordinate-dependent block-matrix,

$$\hat{\varepsilon}(\mathbf{r}) = \begin{pmatrix} \varepsilon_{\alpha\beta}(\mathbf{r}) & 0 \\ 0 & \varepsilon_{zz}(\mathbf{r}) \end{pmatrix}. \tag{2}$$

Here $\varepsilon_{\alpha\beta}(\mathbf{r})$ is a 2×2 Hermitian matrix in the $x-y$ plane. Outside the cylinders it reduces to a scalar, $\varepsilon_b\delta_{\alpha\beta}$ ($\alpha,\beta = x, y$) and inside the cylinders it is given by [40]

$$\varepsilon_{\alpha\beta} = \begin{pmatrix} (x^2\varepsilon_\parallel + y^2\varepsilon_\perp)/r^2 & (xy/r^2)(\varepsilon_\parallel - \varepsilon_\perp) \\ (xy/r^2)(\varepsilon_\parallel - \varepsilon_\perp) & (y^2\varepsilon_\parallel + x^2\varepsilon_\perp)/r^2 \end{pmatrix}. \tag{3}$$

The wave equations for the *E*- and *H*-polarized modes with frequency ω have the following form:

$$\nabla^2 E = \frac{\omega^2}{c^2}\varepsilon_{zz}(\mathbf{r})E, \tag{4}$$

$$\frac{\partial}{\partial x_\alpha}\left(a_{\alpha\beta}\frac{\partial H}{\partial x_\beta}\right) + \frac{\omega^2}{c^2}H = 0, \quad x_\alpha, x_\beta = x, y. \tag{5}$$

Here $E = E(x, y)$ and $H = H(x, y)$ are the amplitudes of the *E* and *H* monochromatic eigenmodes, respectively, and $a_{\alpha\beta}$ is a 2×2 Hermitian matrix with determinant 1:

$$a_{\alpha\beta}(\mathbf{r}) = \frac{\varepsilon_{\alpha\beta(\mathbf{r})}}{\det\|\varepsilon_{\alpha\beta}(\mathbf{r})\|}. \tag{6}$$

The determinant $\det\varepsilon_{\alpha\beta}(\mathbf{r})$ can be written as a product of two eigenvalues. Within the graphite wall of the cylinders this product is $\varepsilon_\parallel\varepsilon_\perp$. Outside the wall it is either $(\varepsilon^{(b)})^2$ (for $\mathbf{r}$ being outside the cylinders) or 1 for the interior region of the hollow cylinder, which is free from the dielectric material.

Since for the *E* polarization the electric field is parallel to the boundaries separating the background from the cylinders, depends only the *zz* component of the dielectric tensor enters in Eq. (4). It means that for this mode the effective dielectric constant is insensitive to in-plane anisotropy. Due to the continuity of the electric field $E(x, y)$ across the cylindrical surfaces, the static dielectric constant of *any* arrangement of parallel cylinders (not necessarily periodic) is given by a simple formula

$$\varepsilon_{\text{eff}}^{(E)} = \bar{\varepsilon}_{zz}, \tag{7}$$

where

$$\bar{\varepsilon}_{zz} = \frac{1}{A_c}\int_{A_c}\varepsilon_{zz}(\mathbf{r})d\mathbf{r}, \tag{8}$$

is the average over the area A_c of the unit cell *zz* component of the tensor (2). For a binary composite

$$\varepsilon_{\text{eff}}^{(E)} = \bar{\varepsilon}_{zz} = f\varepsilon_\perp + (1-f)\varepsilon_b, \tag{9}$$

where *f* is the filling fraction of the component *a*. This effective dielectric constant is thus independent of the direction of propagation and it is simply the weighted average dielectric constant [41].

Anisotropy affects the *H*-polarized mode. To obtain the long-wavelength limit for Eq. (5) we apply the method of plane waves. Using the Bloch theorem and the periodicity of the function $a_{\alpha\beta}(\mathbf{r})$, we get the Fourier expansions,

$$H(\mathbf{r}) = \exp(i\mathbf{k}\cdot\mathbf{r})\sum_{\mathbf{G}} h_{\mathbf{k}}(\mathbf{G})\exp(i\mathbf{G}\cdot\mathbf{r}), \tag{10}$$

$$a_{\alpha\beta}(\mathbf{r}) = \sum_{\mathbf{G}} a_{\alpha\beta}(\mathbf{G})\exp(i\mathbf{G}\cdot\mathbf{r}), \tag{11}$$

where the Fourier coefficients $a_{\alpha\beta}(\mathbf{G})$ are given by

$$a_{\alpha\beta}(\mathbf{G}) = \frac{1}{A_c}\int_{A_c} a_{\alpha\beta}(\mathbf{r})\exp(-i\mathbf{G}\cdot\mathbf{r})d\mathbf{r} = \frac{1}{\varepsilon_\parallel\varepsilon_\perp A_c}\int_a \varepsilon_{\alpha\beta}^{(a)}(\mathbf{r})\exp(-i\mathbf{G}\cdot\mathbf{r})d\mathbf{r} + \frac{\delta_{\alpha\beta}}{A_c}\left[\frac{1}{\varepsilon_b^2}\int_b \exp(-i\mathbf{G}\cdot\mathbf{r})d\mathbf{r} + \int_c \exp(-i\mathbf{G}\cdot\mathbf{r})d\mathbf{r}\right]. \tag{12}$$

Here **G** gives the reciprocal-lattice vectors. Indices *a*, *b*, and *c* at the integrals label the domains of integration — within the graphite walls, within the dielectric matrix, and within the interior of the hollow nanotube, respectively.

Substituting Eqs. (10) and (11) into Eq. (5) we get an eigenvalue problem in **G** space:

$$\sum_{\mathbf{G}'} a_{\alpha\beta}(\mathbf{G}-\mathbf{G}')(k+G)_\alpha (k+G')_\beta\ h_{\mathbf{k}}(\mathbf{G}') = (\omega^2/c^2) h_{\mathbf{k}}(\mathbf{G}). \tag{13}$$

3. The long-wavelength limit

Equation (13) is an infinite set of homogenous linear equations for the eigenfunctions $h_k(\mathbf{G})$. The nontrivial solution is obtained by requiring that the determinant of the coefficients of $h_k(\mathbf{G})$ vanishes. This gives rise to the band structure $\omega = \omega_n(\mathbf{k})$, where *n* is the band index. Being an analytic function, $\omega_n(\mathbf{k})$ may be expanded in a power series of *k* (for any direction of **k**) around $k = 0$. For the lowest (acoustic) band of the spectrum $\omega(0) = 0$ and the expansion starts from the linear term, i.e. $\omega(\mathbf{k}) \propto k$. In the static limit $\omega \to 0$ there can be no magnetic field ($\mathbf{H} = 0$). Therefore all Fourier coefficients $h_k(\mathbf{G})$ must vanish if $k \to 0$. The rates that they approach zero are different: the Fourier coefficients $h_k(\mathbf{G} \neq 0)$ vanish faster than the zero harmonic $h_k(\mathbf{G} = 0)$. To obtain the behavior of $h_k(\mathbf{G})$ we substitute $\mathbf{G} = 0$ in both sides of Eq. (13), divide the both sides by $h_0 = h_{\mathbf{k}}(\mathbf{G} = 0)$ and take the limit $k \to 0$,

$$\omega^2 / c^2 - \bar{a}_{\alpha\beta} k_\alpha k_\beta = \sum_{\mathbf{G}' \neq 0} a_{\alpha\beta}(-\mathbf{G}')\, k_\alpha\ G'_\beta\ h^*_{\mathbf{k}}(\mathbf{G}'). \tag{14}$$

Here $\bar{a}_{\alpha\beta} \equiv a_{\alpha\beta}(\mathbf{G} = 0)$ is the bulk average of the matrix (6) and $h^*_{\mathbf{k}}(\mathbf{G}) = h_{\mathbf{k}}(\mathbf{G}) / h_0$ is the normalized Fourier coefficient. In the long-wavelength limit the coefficients of $h^*_{\mathbf{k}}(\mathbf{G}')$ on the right-hand side are proportional to *k*. In order to make the right-hand side quadratic with *k*, the amplitudes of nonzero harmonics, $h^*_{\mathbf{k}}(\mathbf{G}')$ must be proportional to *k*. Namely, $h^*_k(\mathbf{G} \neq 0) \propto kA_c^{1/2}$. Thus, the Bloch wave (10) can be written as a linear expansion over *k*:

$$H(\mathbf{r}) = \exp(i\mathbf{k}\cdot\mathbf{r}) h_0 [1 + \sum_{\mathbf{G} \neq 0} h^*_{\mathbf{k}}(\mathbf{G}) \exp(i\mathbf{G}\cdot\mathbf{r})]. \tag{15}$$

Since the sum over **G** vanishes linearly with *k*, Eq. (15) shows that the medium becomes homogeneous, i.e., the solution of the wave equation (5) approaches a plane wave.

Now, to calculate the effective dielectric constant (1), we develop a theory of perturbation with respect to a small parameter *ka* ($a \sim A_c^{1/2}$ is a lattice period). In Eq. (13) we keep the linear terms and obtain the following relation:

$$a_{\alpha\beta}(\mathbf{G}) G_\alpha k_\beta + \sum_{\mathbf{G}' \neq 0} a_{\alpha\beta}(\mathbf{G}-\mathbf{G}') G_\alpha G'_\beta\ h^*_k(\mathbf{G}') = 0. \tag{16}$$

The quadratic approximation is given by Eq. (14), which gives another linear relation between the eigenvectors $h^*_{\mathbf{k}}(\mathbf{G})$. Note that this relation is obtained from the eigenvalue problem Eq. (13) for $\mathbf{G} = 0$ and the linear approximation Eq. (16) is obtained for $\mathbf{G} \neq 0$. The linear relations, Eqs. (14) and (16), are the homogenized equations for the Fourier components of the magnetic field. These equations are consistent, if the corresponding determinant vanishes:

$$\det_{\mathbf{G},\mathbf{G}' \neq 0} [\Lambda a_{\alpha\beta}(\mathbf{G}-\mathbf{G}') G_\alpha G'_\beta - a_{\alpha\beta}(\mathbf{G}) a_{\gamma\delta}(-\mathbf{G}') G_\alpha n_\beta n_\gamma G'_\delta] = 0. \tag{17}$$

Here $\mathbf{n} = \mathbf{k} / k$ is the unit vector in the direction of propagation and $\Lambda = (\bar{a}_{\alpha\beta} n_\alpha n_\beta - \varepsilon_{\text{eff}}^{-1})$. Since Eqs. (14) and (16) are homogenous with respect to *k*, the dispersion equation (17) depends only on the inverse effective dielectric constant, $(\omega / ck)^2$. This fact is a manifestation of a general property: At low frequencies an electromagnetic wave has a linear dispersion in a periodic dielectric medium.

Although Eq. (17) is an infinite-order polynomial equation in Λ, it turns out that it has only a *unique* nonzero solution. The fact that the second term in the determinant Eq. (17) is a product of two factors, one of which depends only on **G** and the other only on **G′**, plays a crucial role. Omitting the mathematical details, which can be found in Refs. 21, 25, we give here the final answer for the inverse effective dielectric constant obtained from Eq. (17) as:

$$\frac{1}{\varepsilon_{\text{eff}}^{(H)}(\hat{\mathbf{n}})} = \bar{a}_{\alpha\beta} n_\alpha n_\beta - \sum_{\mathbf{G},\mathbf{G}' \neq 0} a_{\alpha\beta}(\mathbf{G}) a_{\gamma\delta}(-\mathbf{G}')\, n_\beta\, G_\alpha\ n_\gamma\, G'_\delta [a_{\lambda\mu}(\mathbf{G}-\mathbf{G}')\, G_\mu\ G'_\lambda]^{-1}. \tag{18}$$

Here $[...]^{-1}$ implies the inverse matrix in **G** space. Equation (18) is valid for an arbitrary form of the unit cell, geometry of the cylindrical inclusions, material composition of the photonic crystal, and the direction of propagation in the plane of periodicity. In the case when $a_{\alpha\beta}(\mathbf{G}) = \eta(\mathbf{G})\, \delta_{\alpha\beta}$ Eq. (18) is reduced to the formula obtained for isotropic cylinders in Refs. 8, 21 ($\eta(\mathbf{G})$ is the Fourier component of the inverse dielectric constant, $\eta(\mathbf{r}) = 1/\varepsilon(\mathbf{r})$).

The effective dielectric constant Eq. (18) depends on the direction of propagation in the $x - y$ plane and on the details of the photonic crystal structure. For propagation in the plane of periodicity, Eqs. (7), (8), and (18) give a complete solution for the effective dielectric constants of *any* 2D photonic crystal in the low-frequency limit. In what follows we will show how to calculate the *principal dielectric constants*, which give the customary description for anisotropic media in crystal optics [36].

4. Index ellipsoid

As any natural crystal, artificial PC in the long-wavelength limit can be characterized by an index ellipsoid [36]. Taking into account Eq. (7) the equation for this ellipsoid can be written as follows:

$$\frac{x_0^2}{\varepsilon_1}+\frac{y_0^2}{\varepsilon_2}+\frac{z_0^2}{\bar{\varepsilon}_{zz}}=1. \tag{19}$$

Here x_0, y_0, z_0 are three mutually orthogonal directions along which the vectors of the electric field, **E**, and of the displacement, **D**, are parallel to each other. For the *E* mode we have $\mathbf{E}||\mathbf{D}||\hat{\mathbf{z}}$, i.e., the z_0 direction coincides with z axis. In the x–y plane the cross section of the index ellipsoid is given by Eq. (18), which can be rewritten in the canonical form as

$$\frac{1}{\varepsilon_{\text{eff}}^{(H)}(\varphi)}=(\bar{a}_{xx}-A_{xx})\cos^2\varphi+(\bar{a}_{yy}-A_{yy})\sin^2\varphi+$$
$$+(\bar{a}_{xy}-A_{xy})\sin 2\varphi. \tag{20}$$

Here

$$A_{\alpha\beta}=\sum_{\mathbf{G},\mathbf{G}'\neq 0} a_{\alpha\gamma}(\mathbf{G})\, a_{\beta\delta}(-\mathbf{G}')G_\gamma G_\delta'[a_{\lambda\mu}(\mathbf{G}'-\mathbf{G})G_\mu G_\lambda']^{-1},$$
$$\alpha,\beta,\gamma,\delta,\mu,\lambda = x, y. \tag{21}$$

Equation (20) describes a rotated ellipse in the polar coordinates (ρ,φ). The radius $\rho(\varphi)=\sqrt{\varepsilon_{\text{eff}}^{(H)}(\varphi)}$ gives the index of refraction of *H* mode and the angle φ is related to the direction of propagation, $\hat{\mathbf{n}}=(\cos\varphi,\sin\varphi)$. The directions x_0 and y_0 coincide with the semiaxes of the ellipse given by Eq. (20) and the in-plane indices of refraction $\sqrt{\varepsilon_1}$, $\sqrt{\varepsilon_2}$ are given by the lengths of the semiaxes:

$$\varepsilon_1=(\bar{a}_{xx}-A_{xx}\sin^2\theta-A_{yy}\cos^2\theta-A_{xy}\sin 2\theta)^{-1}, \tag{22}$$

$$\varepsilon_2=(\bar{a}_{yy}-A_{xx}\cos^2\theta-A_{yy}\sin^2\theta+A_{xy}\sin 2\theta)^{-1}. \tag{23}$$

The angle of rotation θ of the axes of the ellipse Eq. (20) with respect to some (initially) arbitrary chosen axes x, y is given by the relation

$$\tan 2\theta=\frac{2A_{xy}}{A_{yy}-A_{xx}}. \tag{24}$$

It is the symmetry of the unit cell that determines whether a photonic crystal is uniaxial ($\varepsilon_1=\varepsilon_2$) or biaxial ($\varepsilon_1\neq\varepsilon_2$). Unlike 3D photonic crystals, 2D crystals cannot be isotropic ($\varepsilon_1=\varepsilon_2=\varepsilon_3$). This property is guaranteed by the Wiener bounds ($\varepsilon_{1,2}<\varepsilon_3$) valid at least for in-plane isotropy, namely $\varepsilon_1=\varepsilon_2$ [42]. If the crystal possesses a third- or higher-order rotational axis z, then any second-rank symmetric tensor such as $A_{\alpha\beta}$ Eq. (21), is reduced to a scalar [43], $A_{ik}=A\delta_{\alpha\beta}$ (and $\bar{a}_{\alpha\beta}=\bar{a}\delta_{\alpha\beta}$). Then Eqs. (22) and (23) may be simplified as

$$\varepsilon_1=\varepsilon_2=(\bar{a}-A)^{-1}=$$
$$=\left\{\bar{a}-\frac{1}{2}\sum_{\mathbf{G},\mathbf{G}'\neq 0} a_{\alpha\gamma}(\mathbf{G})\, a_{\alpha\delta}(-\mathbf{G}')G_\gamma G_\delta'[a_{\lambda\mu}(\mathbf{G}'-G)G_\mu G_\lambda']^{-1}\right\}^{-1}. \tag{25}$$

Here $[...]^{-1}$ implies matrix inversion, while $\{...\}^{-1}$ means «reciprocal». This compact formula gives the principal dielectric constant (associated with the plane of periodicity) of a uniaxial photonic crystal. The optical axis coincides with the axis z, which is to say that birefringence is absent for a single direction of propagation — the direction parallel to the cylinders. For propagation in this direction (with $\mathbf{E}\perp\hat{\mathbf{z}}$) the phase velocities of the «ordinary» and «extraordinary» waves are the same, $\omega/k=c/\sqrt{\varepsilon_1}$, with ε_1 given by Eq. (25). Of course, for any direction of propagation the «ordinary wave» propagates with the same speed, $c/\sqrt{\varepsilon_1}$, by definition. Because this velocity is always less than the velocity $c/\sqrt{\bar{\varepsilon}_{zz}}$ of the «extraordinary wave» (with $\mathbf{E}||\hat{\mathbf{z}}$) that propagates in the plane of periodicity, we may conclude that uniaxial 2D photonic crystals are necessarily «positive» optically anisotropic crystals.

5. Uniaxial and biaxial photonic crystals of solid graphite cylinders

In this section, we study 2D photonic crystals of solid graphite cylinders arranged in square and rectangular lattices. In Cartesian coordinates the dielectric function of a carbon cylinder is given by Eq. (3). For rectangular and square lattices with circular cylinders the semiaxes of the index ellipsoid are directed along the basic lattice vectors. Because of the cylindrical symmetry of the inclusions, the off-diagonal elements of the tensor $a_{\alpha\beta}(\mathbf{G})$ vanish [44]. The diagonal elements for hollow cylinders with outer and inner radii R and γR, respectively ($0\le\gamma\le 1$), have the following form:

$$a_{xx}(0)=\left(\varepsilon_b^{-1}+\frac{\pi R^2(1-\gamma^2)}{2A_c}\right)(\varepsilon_\parallel^{-1}+\varepsilon_\perp^{-1}-2\varepsilon_b^{-1}),$$
$$a_{xx}(\mathbf{G})=(2\pi/(A_cG^2))\{GR(\varepsilon_b^{-1}-\varepsilon_\perp^{-1})\times$$
$$\times[\gamma J_1(\gamma GR)-J_1(GR)]+(\varepsilon_\parallel^{-1}-\varepsilon_\perp^{-1})J_0(GR)-J_0(\gamma GR)\}. \tag{26}$$

The diagonal element $a_{yy}(\mathbf{G})$ is obtained from Eq. (26) by the replacement $\varepsilon_\perp\leftrightarrow\varepsilon_\parallel$.

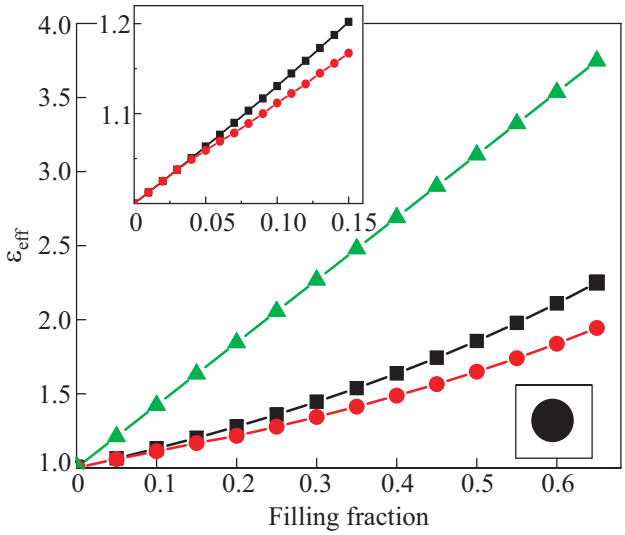

Fig. 2. In-plane effective dielectric constant for the H mode for uniaxial PC of solid graphite cylinders with $\varepsilon_{\parallel} = 1.8225$ and $\varepsilon_{\perp} = 5.226$ in air, $\varepsilon_b = 1$ (circles). Straight line (triangles) is the effective dielectric constant $\bar{\varepsilon}_{zz}$ for the E mode, Eq. (8). The squares show the results of the Maxwell-Garnett approximation (27). Inset shows the region of very small filling fractions.

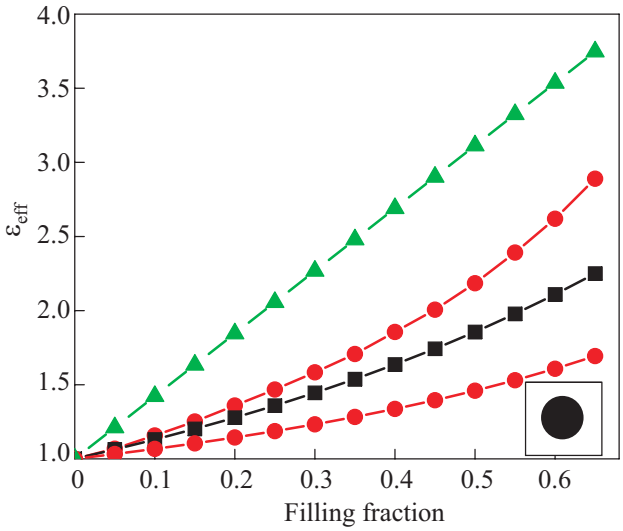

Fig. 3. A plot of the principal effective dielectric constants for the photonic crystal of solid graphite cylinders arranged in a rectangular lattice. In this case the effective medium is a biaxial crystal with all three different principal dielectric constants. The larger (smaller) in-plane dielectric constant ε_1 (ε_2) corresponds to the direction of the vector **E** along the short (long) side of the rectangle. The Maxwell-Garnett dielectric constant is shown by the squares. The triangles show $\bar{\varepsilon}_{zz}$.

For solid cylinders, i.e. $\gamma \equiv 0$. The circles in Fig. 2 show the effective dielectric constant, given by Eq. (20), of the H mode as a function of the filling fraction, $f = \pi R^2 / A_c$, for the uniaxial photonic crystal with a square lattice. The number of **G** values (plane waves) considered in this calculation was 1200, which provides a good convergence in Eq. (25). In accordance with the Wiener bounds, the dielectric constant Eq. (7) for the extra-ordinary wave (E mode) (shown by triangles in Fig. 2) is always larger than that for the ordinary wave (H mode), i.e., the effective medium is an uniaxial positive crystal.

For a long time, there have been extensive efforts to construct effective medium theories for inhomogeneous media. The well-known Maxwell-Garnett approximation [45] gives good results for very small filling fractions ($f << 1$ or $1 - f << 1$) but it fails otherwise. It also does not take into account the microstructure of the inhomogeneous medium. To check the validity of the Maxwell-Garnett approximation, we plot in Fig. 2 (squares) the effective dielectric constant proposed in Ref. 40:

$$\varepsilon_{MG}^{(H)} = \frac{\varepsilon_{\parallel} + \Delta + f(\varepsilon_{\parallel} - \Delta)}{\varepsilon_{\parallel} + \Delta - f(\varepsilon_{\parallel} - \Delta)}. \qquad (27)$$

Here $\Delta = \sqrt{\varepsilon_{\parallel} / \varepsilon_{\perp}}$. One can see that for all filling fractions the Maxwell-Garnett approximation gives overestimated values for the effective dielectric constant. For a very dilute system, $f < 0.07$, the Maxwell-Garnett approximation gives results that are practically indistinguishable from the exact ones (see inset in Fig. 2). For the close-packed array of cylinders the Maxwell-Garnett approximation overestimates the dielectric constant by about 25%.

In Fig. 3 we plot two principal dielectric constants for the biaxial PC of solid carbon cylinders with a rectangular unit cell. The ratio of the sides of the rectangle is 1:2. The difference between the two dielectric constants increases with the filling fraction, giving rise to a higher anisotropy of the corresponding effective medium. The Maxwell-Garnett approximation Eq. (27), which does not take into account the anisotropy of the unit cell, gives the values for ε_{MG} that lie between the two principal values, $\varepsilon_1 < \varepsilon_{MG} < \varepsilon_2$.

6. Uniaxial photonic crystal of carbon nanotubes

In our model we consider the carbon nanotubes as hollow graphite cylinders. In the experimental study [30] of the dielectric properties of carbon nanotubes the outer radius of the cylinders was approximately $R = 5$ nm. The nanotubes formed a thin film and they were oriented along a specific direction. Although the nanotubes were not necessarily arranged periodically, one can assume that they formed almost a regular lattice, since the nanotube density is about 0.6–0.7 which is near the value of $f_c = \pi / 4 \approx 0.785$ for a close-packed structure. Thus, the separation between the nanotubes (the period of the square lattice d) slightly exceeds $2R$, and in Ref. 40 it was estimated to be $d = 10.15$ nm. The inner radius $\gamma R = 0.25$–2 nm was evaluated from the amount of electro-

magnetic absorption for the E-polarized light [40]. The four parameters f, R, γ, and $A_c = a^2$ are not independent but related by the formula

$$f = \pi R^2 (1-\gamma^2) / A_c. \qquad (28)$$

Substituting the aforementioned parameters of the square unit cell into this formula allows one to check that they are self-consistent. It is worthwhile to mention that the background material in the experiment [30] is not air but the host material Delrin or Teflon with $\varepsilon_b > 1$. Since neither the density of the host material nor its dielectric constant is known, one cannot expect very good agreement between the experimental results [30] and theory. In all theoretical considerations it was assumed that $\varepsilon_b = 1$. Because of this lack of experimental data, the effective medium theories [32,40,46] and the results shown in Fig. 2 give lower values for ε_{eff} than that observed in the experiment [30].

It is obvious that the inner cavity reduces the permittivity of an isolated nanotube as compared to a solid graphite cylinder of the same size. It was argued [40] that for a periodic arrangement the effect of the inner cavity is less than that for a single cylinder and even can be ignored, if the ratio between the inner and outer radii γ does not exceed 0.4. This conclusion was supported by comparing the results of the Maxwell-Garnett approximation Eq. (27) and numerical band structure calculations. In Fig. 4 we plot the dielectric constant for a square lattice of hollow carbon nanotubes and compare the exact results obtained from Eqs. (20), (21), and (26) (shown by the circles) with the results given by the Maxwell-Garnett approximation (squares). One can see that, for the same outer radius, the effective dielectric constant drops with an increase of the inner radius. Thus, if the outer radius is fixed, the dependence on the inner radius cannot be ignored, even in the Maxwell-Garnett approximation. However, the effective dielectric constants exhibits much less sensitivity to the internal radius if it is plotted against filling fraction, Fig. 5.

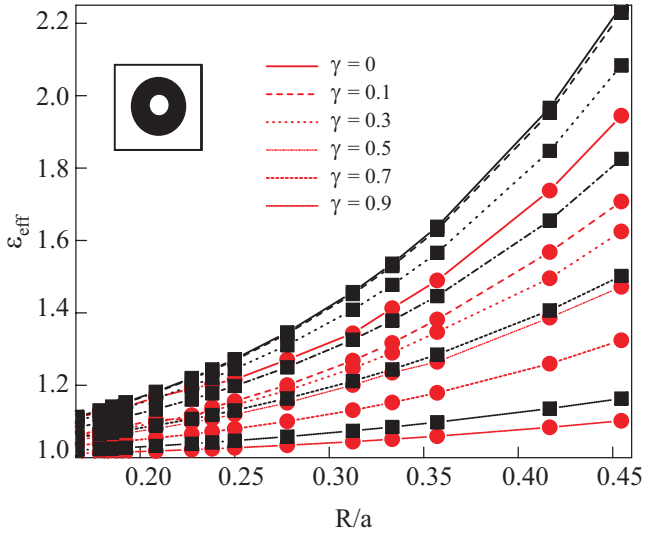

Fig. 4. The plot of the effective dielectric constant for square lattice of carbon nanotubes versus the outer radius for tubes with different ratios of the inner and outer radii, $\gamma = 0.1$, 0.3, 0.5, 0.7, 0.9. The exact results are shown by circles and the results of the Maxwell-Garnett approximation are shown by squares.

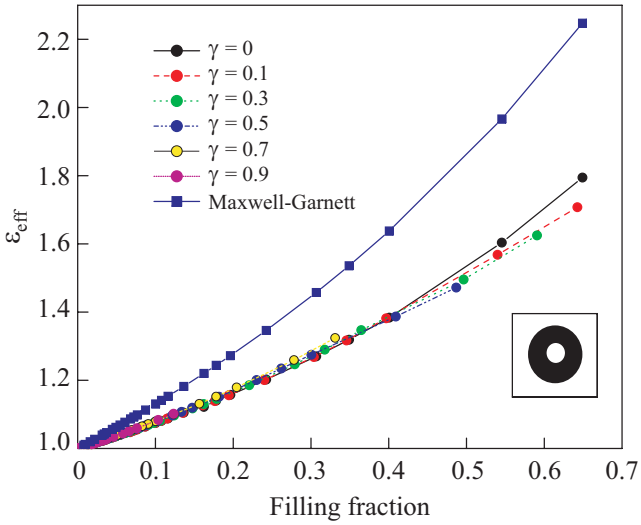

Fig. 5. A graph of the effective dielectric constant for a square lattice of carbon nanotubes versus filling fraction for tubes with different ratios of the inner and outer radii, $\gamma = 0.1$, 0.3, 0.5, 0.7, 0.9. The exact results are shown by circles and the Maxwell-Garnett approximation is shown by squares.

In the Maxwell-Garnett approximation (27) there is no dependence on the parameter γ, therefore, this approximation is represented by a single curve in Fig. 5. Here, only the total amount of the dielectric material is important (i.e., the filling fraction of the carbon), but not the topology of the cylinders. In our exact theory the effective dielectric constant depends on the details of the microstructure of the photonic crystal, but as far as the filling fraction is concerned, the topology plays a much less important role. Since the cylinder is uniquely determined by either two parameters out of three, R, γ, and f, the curves in Fig. 5 may cross each other. This means that at the crossing point the values of f and γ correspond to the same hollow cylinder. This can be easily seen from Eq. (28).

7. Conclusions

We calculated the low-frequency dielectric tensor for 2D photonic crystal of optically anisotropic parallel cylinders arranged in a periodic lattice in the perpendicular plane. The exact analytical formula for the principal values of the dielectric tensor was obtained. The results are

applied for the periodic arrangement of carbon nanotubes which are rolled up from uniaxial graphite crystal with static values of the dielectric tensor $\varepsilon_{\|} = 1.8225$ and $\varepsilon_{\perp} = 5.226$. It was shown that the interior (vacuum) region of the nanotubes has a small effect on the dielectric properties of the photonic crystal and can be ignored. Although we are interested in the static dielectric tensor, it is clear that the developed long-wavelength limit approach remains valid, even for optical frequencies since the period of the lattice of carbon nanotubes $d = 10$ nm is much less than the optical wavelength $\lambda \approx 500$ nm. To calculate the dynamic dielectric tensor, one has to substitute in the general formula Eq. (18) the corresponding frequency-dependent values for $\varepsilon_{\|}$ and $\varepsilon_{\perp}$. Of course at finite frequencies Eq. (18) gives the real part of the dielectric function. Calculations of the imaginary part require a generalization of the presented theory. This result will be reported elsewhere.

The exact theory presented here allows a calculation of the effective dielectric constant of carbon nanotubes imbedded in a gas. Due to high absorbability of nanotubes, the concentration of gas in the interior region of the nanotubes may be different from that in the atmosphere. This leads to slightly different dielectric constants of the material in the interior and exterior regions of the cylinders. This effect can be registered by precise measurements of the shift of the resonant frequency of a resonant cavity [47]. Thus, the proposed theory may find applications in the microwave detection of Poisson gases in the atmosphere.

One more interesting application of carbon nanotube photonic crystal is related to its huge anisotropy of the effective dielectric constant. Recently Artigas and Torner [11] demonstrated that the electromagnetic surface wave (Dyakonov wave [38]) can propagate along the surface of a photonic crystal with high optical anisotropy. This wave propagates in a lossless dielectric medium and decays much slower than surface plasmon-polariton. Since crystals with huge optical anisotropy are rare in nature, carbon nanotube photonic crystals may be considered as a promising material for integrated photonic circuits where information is transmitted by surface modes.

Acknowledgment

This work is supported by the US Department of Energy grant # DE-FG02-06ER46312.

1. E. Yablonovitch and T.J. Gmitter, *Phys. Rev. Lett.* **63**, 1950 (1989).
2. see, e.g., *Roadmap to Photonic Crystals*, S. Noda and T. Baba (eds.), Kluwer, Boston (2003).
3. E. Yablonovitch, *Phys. Rev. Lett.* **58**, 2059 (1987).
4. K. Sakoda, *Optical Properties of Photonic Crystals*, Springer-Verlag, Berlin (2001).
5. C. Jamois, R.B. Wehrspohn, L.C. Andreani, C. Hermann, O. Hess, and U. Gösele, *Photonics and Nanostructures — Fundamentals and Applications* **1**, 1 (2003).
6. C. Luo, M. Ibanescu, E.J. Reed, S.G. Johnson, and J.D. Joannopoulos, *Phys. Rev. Lett.* **96**, 043903 (2006).
7. J.B. Pendry and D.R. Smith, *Phys. Today* **57**, 37 (2004); V.M. Shalaev, *Nature Photonics* **1**, 41 (2007).
8. P. Halevi, A.A. Krokhin, and J. Arriaga, *Phys. Rev. Lett.* **82**, 719 (1999).
9. V.A. Podolskiy and E.E. Narimanov, *Phys. Rev.* **B71**, 201101(R) (2005).
10. D. Artigas and L. Torner, *Phys. Rev. Lett.* **94**, 013901 (2005).
11. M. Sahimi, *Heterogeneous Materials*, Springer, New York (2003); P. Kuchment, *The Mathematics of Photonic Crystals*, in: *Mathematical Modeling in Optical Science*, G. Bao, L. Cowsar, and Wen Masters (eds.), SIAM, Philadelphia (2001), Vol. 22, p. 207; M. Birman and T. Suslina, *Operator Theory Adv. Appl*. **129**, 71 (2001).
12. P. Halevi, A.A. Krokhin, and J. Arriaga, *Appl. Phys. Lett.* **75**, 2725 (1999).
13. R. Tao, Z. Chen, and P. Sheng, *Phys. Rev.* **B41**, 2417 (1990).
14. D.J. Bergman and K.J. Dunn, *Phys. Rev.* **B45**, 13262 (1992).
15. S. Datta, C.T. Chan, K.M. Ho, and C.M. Soukoulis, *Phys. Rev.* **B48**, 14936 (1993).
16. I.H.H. Zabel and D. Stroud, *Phys. Rev.* **B48**, 5004 (1993); Zh.-Yu. Li, J. Wang, and B.-Yu. Gu, *Phys. Rev.* **B58**, 3721 (1998).
17. K. Ohtaka, T. Ueta, and Y. Tanabe, *J. Phys. Soc. Jpn*. **65**, 3068 (1996).
18. N.A. Nicorovici, R.C. McPhedran, and L.C. Botten, *Phys. Rev. Lett.* **75**, 1507 (1995); N.A. Nicorovici and R.C. McPhedran, *Phys. Rev.* **E54**, 1945 (1996); R.C. McPhedran, N.A. Nicorovici, and L.C. Botten, *J. Electom. Waves Appl*. **11**, 981 (1997).
19. P. Lalanne, *Appl. Optics* **27**, 5369 (1996); *Phys. Rev.* **B58**, 9801 (1998).
20. P. Halevi, A.A. Krokhin, and J. Arriaga, *Phys. Rev. Lett.* **86**, 3211 (2001).
21. A.A. Krokhin, P. Halevi, and J. Arriaga, *Phys. Rev.* **B65**, 115208 (2002).
22. A.A. Krokhin, L.N. Gumen, H.J. Padilla Martinez, and J. Arriaga, *Physica* **E17**, 398 (2003).
23. J. Arriaga, A.A. Krokhin, and P. Halevi, *Physica* **E17**, 436 (2003).
24. A.A. Krokhin, J. Arriaga, and L.N. Gumen, *Phys. Rev. Lett.* **91**, 264302 (2003).
25. A.A. Krokhin and E. Reyes, *Phys. Rev. Lett.* **93**, 023904 (2004).
26. E. Reyes, A.A. Krokhin, and J. Roberts, *Phys. Rev.* **B72**, 155118 (2005).
27. A.A. Krokhin, E. Reyes, and L. Gumen, *Phys. Rev.* **B75**, 045131 (2007).
28. D. Felbacq, *J. Math. Phys*. **43**, 52 (2002).
29. X. Hu and C.T. Chan, *Phys. Rev. Lett.* **95**, 154501 (2005).
30. W.A. de Heer, W.S. Bacsa, A. Châtelain, T. Gerfin, R. Humphrey-Baker, L. Forro, and D. Ugarte, *Science* **268**, 845 (1995).

31. F. Bommeli, L. Degiorgi, P. Wachter, W.S. Bacsa, W.A. de Heer, and L. Forro, *Solid State Commun*. **99**, 513 (1996).
32. K. Kempa, B. Kimball, J. Rybczynski, Z.P. Huang, P.F. Wu, D. Steeves, M. Sennett, M. Giersig, D.V.G.L.N. Rao, D.L. Carnahan, D.Z. Wang, J.Y. Lao, W.Z. Li, and Z.F. Ren, *Nano Letters* **3**, 13 (2003).
33. X. Wang and K. Kempa, *Appl. Phys. Lett.* **84**, 1817 (2004).
34. Y. Wang, X. Wang, J. Rybczynski, D.Z. Wang, K. Kempa, and Z.F. Ren, *Appl. Phys. Lett.* **86**, 153120 (2005).
35. V.G. Veselago, *Sov. Phys. Usp*. **10**, 509 (1968); J.B. Pendry, *Phys. Rev. Lett.* **85** 3966 (2000).
36. M. Born and E. Wolf, *Princilples of Optics*, 7th ed., Cambridge University Pres, Cambridge (1999).
37. *Handbook of Optical Constant of Solids*, E.D. Palik (ed.), Academic, Orlando (1991).
38. M.I. Dyakonov, *Sov. Phys. JETP* **67**, 714 (1988).
39. A.A. Krokhin, A. Neogi, and D. McNeil, *Phys. Rev.* **B75**, 235420 (2007).
40. F.J. García-Vidal, J.M Pitarke, and J.B. Pendry, *Phys. Rev. Lett.* **78**, 4289 (1997).
41. R. Fuchs, *Phys. Rev.* **B11**, 1732 (1975); D.J. Bergman, *ibid.* **14**, 4304 (1976); R. Fuchs and F. Claro, *ibid.* **39**, 3875 (1989).
42. O. Wiener, *Abh. Sächs. Akad. Wiss. Leipzig Math.-Naturwiss*. Kl. **32**, 509 (1912).
43. L.D. Landau, E.M. Lifshitz, and L.P. Pitaevskii, *Electrodynamics of Continuous Media*, 2nd ed., Pergamon, Oxford (1984).
44. The off-diagonal elements are proportional to the integral $\int_0^{\pi} \sin\theta \cos\theta \exp(-iGr\cos\theta)\, d\theta$, which vanishes identically.
45. J.C. Maxwell-Garnett, *Philos. Trans. R. Soc*. **203**, 385 (1904).
46. W. Lü, J. Dong, and Z.-Y. Li, *Phys. Rev.* **B63**, 033401 (2000).
47. A. Anand, J.A. Roberts, F. Naab, J.N. Dahiya, O.W. Holland, and F.D. McDaniel, *Select Gas Absorption in Carbon Nanotubes Loading a Resonant Cavity to Sence Airborne Toxins Gases*, Nuclear Instruments and Methods B, Elsivier (2005).